Geochemistry, Geophysics, Geosystems

RESEARCH ARTICLE
10.1029/2020GC009557

Key Points:

- Enamel of fossil elephants is well-preserved from diagenesis.
- Electron microscopy, X-ray diffraction, isotope analysis and elemental analysis give the composition and ultrastructure of enamel.

Supporting Information:

Supporting Information may be found in the online version of this article.

Correspondence to:

M. Epple and R. Patnaik,
matthias.epple@uni-due.de
rajeevpatnaik@gmail.com

Citation:

Białas, N., Prymak, O., Singh, N. P., Paul, D., Patnaik, R., & Epple, M. (2021). Teeth of past and present elephants: Microstructure and composition of enamel in fossilized proboscidean molars and implications for diagenesis. *Geochemistry, Geophysics, Geosystems*, *22*, e2020GC009557. https://doi.org/10.1029/2020GC009557

Received 25 NOV 2020
Accepted 31 MAR 2021

Teeth of Past and Present Elephants: Microstructure and Composition of Enamel in Fossilized Proboscidean Molars and Implications for Diagenesis

Nataniel Białas[1], Oleg Prymak[1], Ningthoujam Premjit Singh[2], Debajyoti Paul[3], Rajeev Patnaik[2], and Matthias Epple[1]

[1]Inorganic Chemistry and Center for Nanointegration Duisburg-Essen (CeNIDE), University of Duisburg-Essen, Essen, Germany, [2]Department of Geology, Panjab University, Chandigarh, India, [3]Department of Earth Sciences, Indian Institute of Technology, Kanpur, India

Abstract Enamel as hardest biological tissue remains unaltered for millions of years and is therefore an excellent archive for studies on paleodiet, paleoecology, paleoclimate, paleoenvironment, biomechanical, and evolutionary studies. However, diagenetic alterations can influence such interpretations and therefore we analyzed the microstructure and composition (elemental and stable isotopic) of fossil and extant proboscidean teeth to study the extent of diagenesis in them. We report for the first time on the enamel microstructure data of the Indian elephantiformes *Anancus*, *Stegodon*, *Elephas*, and *Palaeoloxodon* besides analyzing *Gomphotherium* and *Deinotherium* from new formations. Furthermore, we compare their microstructure with those of the primitive African taxa of *Moeritherium* and *Palaeomastodon*. Our results from depth-related elemental composition and oxygen isotope ratios of enamel phosphate and carbonate indicate no or only negligible modification. There is also a lack of age-dependency of these minor alterations within the fossils collected from Siwaliks of the Himalayan Foreland Basin. Overall, our study indicates that diagenesis has not played any significant role on the samples studied here and are therefore well suited for chemical and paleontological studies and proxy for paleoclimate and paleoenvironment reconstruction.

1. Introduction

Teeth play a fundamental role in the life of vertebrates. Their main functions are catching prey, shredding and mastication of food (as part of the digestive system), and defense from predators. Teeth contain dentin as softer, bone-like material in the tooth interior and enamel as highly mineralized material on the tooth surface (Teaford et al., 2000). The latter is also known to be the hardest biological material found in nature.

Enamel has a distinct prismatic microstructure and is highly resistant to chemical alteration during the process of fossilization or diagenesis. It consists mostly of calcium phosphate (~96 wt%), water (~3 wt%), and organic matter (~1 wt%) (Dorozhkin & Epple, 2002). In comparison, dentin is made of ~70–75% calcium phosphate, ~5%–10% water and ~20% organic matter (Dorozhkin & Epple, 2002). Carbonated hydroxyapatite $Ca_{10}(PO_4,CO_3)_6(OH)_2$ (HAp) is the main tooth mineral in vertebrates, with some structural carbonate ions (CO_3^{2-}) substituting the dominant phosphate (PO_4^{3-}) ions (Daculsi et al., 1990; LeGeros, 1981; LeGeros et al., 1968). This biologically occurring apatite is often denoted as bioapatite, a term that we will use in the following. However, its crystallographic nature is still based on the hydroxyxapatite structure (Dorozhkin & Epple, 2002). Bioapatite in bone and teeth contains between 3 wt% and 7 wt% carbonate (Dorozhkin & Epple, 2002). As a notable exception, teeth of cartilaginous fish (e.g., sharks, and rays) consist of the mineral fluorapatite $Ca_{10}(PO_4)_6F_2$ (FAp) (Daculsi & Kerebel, 1980; Enax et al., 2012; LeGeros & Suga, 1980; Luebke et al., 2015; Luebke et al., 2017). Enamel can be described as a highly compact tissue with tiny pore space, distinct prismatic microstructure, and the presence of long hydroxyapatite crystallites (>1 μm). In contrast, dentin is a porous tissue with small crystallites (<0.1 μm) and more organic matter, which makes it less resistant to geochemical alterations than enamel (Kohn et al., 1999). The high level of mineralization in enamel ensures the durability of prismatic microstructure which remains almost unaltered during fossilization and shows low susceptibility to structural changes related to diagenetic origin (Tabuce et al., 2007). Therefore, fossilized teeth are an attractive research model in paleontology. They provide information about the animal (i.e., age, diet, and taxonomy), paleoclimate and its influence on the animal (e.g., pollution

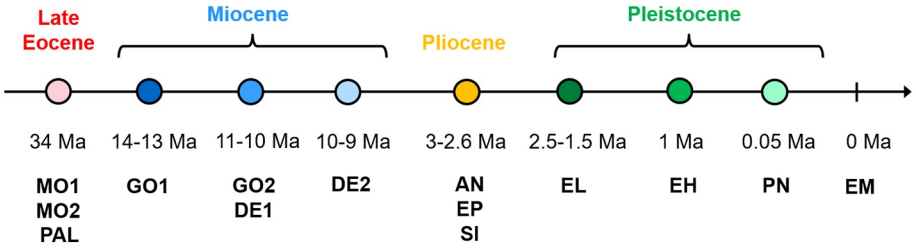

Figure 1. Age of the studied fossil elephants on a geologic time scale. For details see Table 1. Ma: Millions of years.

exposure), animal migration patterns and evolutionary changes (Ferretti, 2003; Humphrey, 2017; Kohn et al., 1999; Locke, 2008; McCollum & Sharpe, 2001).

Nowadays, the Earth is inhabited by three elephant species, that is, the African bush elephant (*Loxodonta africana*), the African forest elephant (*L. cyclotis*), and the Asian elephant (*Elephas maximus*) (Roca et al., 2001). They are the only remaining representatives of the large and well developed past order *Proboscidea* which originated in Africa-Arabia in the early Paleocene (~65 Ma) and diversified in the Eocene (Maglio, 1973). Some of the early proboscidean from Africa include *Eritherium* from Paleocene and *Phosphatherium* from early Eocene (Gheerbrant, 2009; Gheerbrant et al., 1998, 2012). The Fayum Basin of Egypt has yielded other early proboscideans including *Moeritherium* and *Palaeomastodon*. From the taxonomical point of view, proboscideans are related to the aquatic sirenians and terrestrial hyracoids (Liu et al., 2008; Van der Made, 2010). Proboscideans were also key herbivores in Neogene ecosystems (~23–2.6 Ma) as several large-bodied elephant species occupied the landscape (Wu et al., 2018). In the early Miocene (~23 Ma), due to plate tectonics, a terrestrial connection (known as the "*Gomphotherium* Land Bridge") between Africa-Arabia and Eurasia was formed, which led to faunal exchange with the previously isolated Tethys continents (Rögl, 1998). The first proboscideans, like *Prodeinotherium* (~23 Ma) and *Gomphotherium* (~22 Ma), could then enter Eurasia and reach the Indian subcontinent (Patnaik, 2016; Van der Made, 2010). The endemic evolution of the gomphotheres in Asia likely led to the emergence of *Anancus* and *Stegodon* (Van der Made, 2010). Plio-Pleistocene waves of African immigrant elephants include *Elephas* followed by *Palaeoloxodon*.

In proboscideans, several types of enamel have been described, both prismatic and prismless. Among prismatic enamel, three different structural types can be distinguished. The 3D enamel (3DE) is irregular and has no precise structural units. It is composed of parallel prisms that come out of the enamel-dentin junction (EDJ) and tend to form bundles of various thickness (~15–20 prisms), which run in different directions. In Hunter-Schreger-Bands (HSB), parallel prisms form layers of various thickness at an angle to prisms in adjacent layers. The radial enamel (RE) consists of parallel prisms radially directed from the EDJ, whereas prismless enamel (PE/PLE) consists of parallel apatite crystallites. HSB, RE, and PE are typical for placental mammals, and 3DE is typical for proboscideans (Ferretti, 2003). Schmelzmuster" is the accepted term to describe the distribution of the various enamel types within the tooth (Koenigswald & Sander, 1997). There are three types of prism cross-section patterns: Prism pattern 1 refers to prisms with complete boundaries arranged horizontally in relation to the tooth growth axis; pattern 2 shows arced shaped prism cross-section where prisms are arranged in vertical rows separated by inter-row sheets, whereas arc-shaped pattern 3 prisms are arranged in horizontal rows (Boyde, 1967). Most proboscideans show pattern 3 prism cross-sections, which in turn basically consist of three types: Key-hole, fan-shaped, and ginko-leaf pattern.

The biomechanical properties of enamel are determined by the function of the tooth (Ben-Zvi et al., 2019; Eder et al., 2018; Enax et al., 2013; Vollrath et al., 2018). Prism decussation in 3DE and HSB increases the enamel resistance to fracture, whereas the perpendicular orientation of prisms to the masticatory surface of the tooth in RE enhances resistance to abrasive wear (Ferretti, 2007). In the dental evolution of proboscideans, a clear enamel-thinning trend was observed (Ferretti, 2007). Furthermore, their grinding teeth evolved from low-crowned molars ("mastodont-like") to high-crowned teeth ("elephant-like") as an adaptation to the increasing role of abrasive food (grass) in their diet (Wu et al., 2018).

Table 1
List of all Elephant Tooth Enamel Samples Investigated in This Study

Sample key	Taxa	Stratigraphy	Location	Age/millions of years
MO1	*Moeritherium* sp.	Late Eocene, Birket Qarun Formation	Fayum, Egypt	~34
MO2	*Moeritherium* sp.	Late Eocene, Birket Qarun Formation	Fayum, Egypt	~34
PAL	*Palaeomastodon*	Late Eocene, Birket Qarun Formation	Fayum, Egypt	~34
RB41	*Rhinocerotidae*	Middle Miocene, Chinji Formation	Bassi (Ramnagar), India	~14–13
GO1	*Gomphotherium* sp.	Middle Miocene, Chinji Formation	Kulwanta (Ramnagar), India	~14–13
GO2	*Gomphotherium* sp.	Late Miocene, Khari Nadi Formation	Tapar (Kutch), India	~11–10
DE1	*Deinotherium* sp.	Late Miocene, Khari Nadi Formation	Tapar (Kutch), India	~11–10
DE2	*Deinotherium* sp.	Late Miocene, Dhok Pathan Formation	Haritalyangar, India	~10–9
AN	*Anancus* sp.	Late Pliocene, Tatrot Formation	Khetpurali, India	~3–2.6
SI	*Stegodon insignis*	Late Pliocene, Tatrot Formation	Nathunala, India	~3–2.6
EP	*Elephas platycephalus*	Late Pliocene, Tatrot Formation	Quranwala, India	~3–2.6
EL	*Elephas* sp.	Early Pleistocene, Pinjor Formation	Quranwala, India	~2.5–1.5
EH	*Elephas hysudricus*	Middle Pleistocene, Boulder Conglomerate	Dudhgarh, India	~1
PN	*Palaeoloxodon namadicus*	Late Pleistocene, Surajkund Formation	Hoshnagabad, India	~0.05
EM	*Elephas maximus*	Recent	Simlipal, India	0

It has been established that proboscideans developed their teeth from low-crowned (with thick, undifferentiated enamel) to high-crowned (with thin, differentiated enamel) to adapt to a shift in vegetation in the Late Miocene from low to high abrasiveness, that is, containing high amounts of silica, which evolved due to climate change (Bertrand, 1988; Kozawa, 1985; Maglio, 1973; Pfretzschner, 1994; Tabuce et al., 2007; Koenigswald et al., 1993). In the Indian subcontinent such a dietary shift among the proboscideans has been observed around 8–7 Ma (Patnaik et al., 2019). Therefore, fossilized teeth can provide valuable information on the paleoclimate and paleovegetation patterns prevailing when the animal was alive.

The Neogene and Quaternary deposits of India that include the Siwaliks (foothills of the Himalayas), Kutch (Western India, Gujarat), and Narmada Valley (Central India) are well known for the late proboscidean remains.

This work presents a comprehensive study on the chemical composition and microstructure of ten enamel samples of fossilized molar teeth of extinct elephant ancestors collected from the Neogene and Quaternary deposits of India, besides one enamel sample of the modern elephant *Elephas maximus*. We also analyzed three enamel fragment samples of *Moeritherium* and *Palaeomastodon* collected from Fayum Basin, Egypt, for comparison. Microstructure and composition were analyzed in detail by advanced chemical and microscopic methods, that is, atomic absorption spectroscopy (AAS), ion-selective potentiometry (ISP), ultraviolet spectroscopy (UV/VIS), infrared spectroscopy (IR), thermogravimetry (TG), scanning electron microscopy (SEM), energy-dispersive X-ray spectroscopy (EDX), and X-ray powder diffraction (XRD), including Rietveld refinement. Additionally, we obtained the stable oxygen isotope ratio of PO_4^{3-} ($\delta^{18}O$-PO_4^{3-}) and correlated the results with the $\delta^{18}O$-CO_3^{2-} values of HAp in selected associated samples (eight proboscidean and one rhinoceratid) to determine the extent of diagenetic alteration in fossilized teeth.

2. Materials and Methods

All samples were identified, and provided by R. Patnaik (for full sample descriptions, see Table 1 and Table 4). Most fossilized teeth were found in the Indian part of the Siwalik Hills (also known as Siwaliks) (Figure 2). These are foothills of the Himalayas, which are well known for the occurrence of Miocene-Pleistocene vertebrate fossils (Abbas et al., 2018, 2019; Kumar et al., 2017; Patnaik et al., 2018). These fossils are extremely valuable in studies on paleoclimate, paleoenvironment, and geological evolution of the Himalayas.

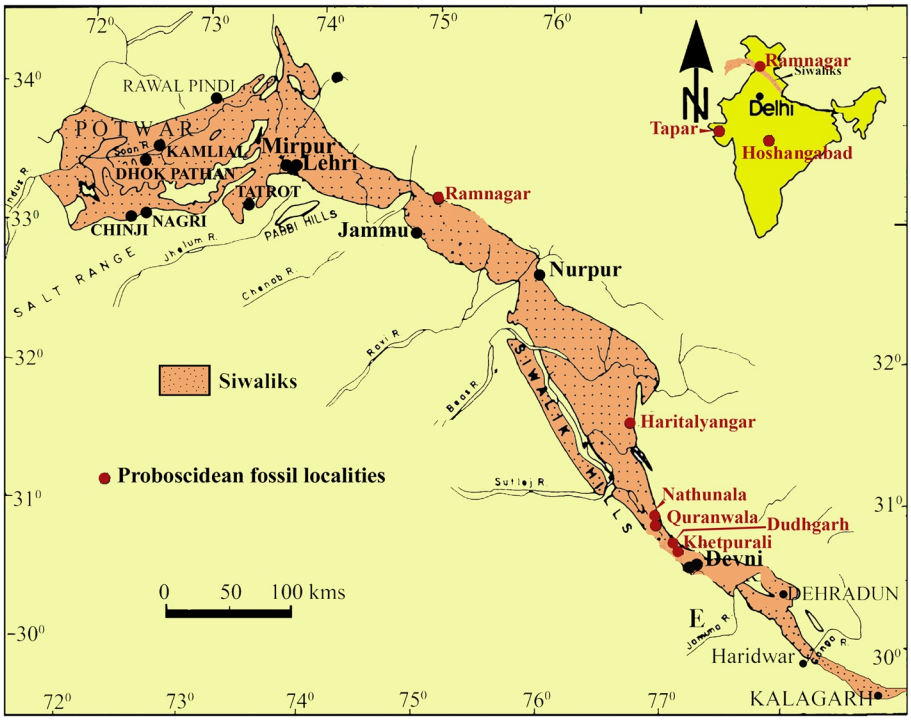

Figure 2. Map of India and Siwaliks showing proboscidean fossil localities.

Pulverized enamel, obtained by precise drilling of the enamel samples with a jewelry diamond drill (Proxxon, FBS 230/E), was used for combustion analysis, AAS, ISP, UV/VIS, IR, TG, and XRD. Whole enamel samples were used for SEM and energy-dispersive EDX. For SEM and EDX analyses, vertical (parallel to the mesio-distal tooth axis) and tangential (parallel to the tooth enamel surface) sections of the enamel samples were prepared with a Buehler Isomet 1,000 Precision Cutter.

Freshly broken and etched samples were also observed by SEM. The samples were polished (ATM, Saphir 520) with a water-based polycrystalline diamond suspension (ATM GmbH, grain size 3 μm), etched with 5% nitric acid (diluted from 65%, Fisher) in absolute ethanol (Fisher) for 1 min, washed with double-distilled water in an ultrasonic bath (Bandelin Sonorex^{TM}, RK-100) for 1 min, rinsed with ethanol, dried, and sputter-coated with gold and palladium (80:20) for 30 s (Cressington, Sputter Coater 108). The microstructure of enamel and the local distribution of elements in the enamel were then analyzed by SEM (Thermo Scientific, ESEM Quanta™ 400 FEG) combined with energy-dispersive EDX (detector type: SUTW-sapphire, resolution: 128.81, Lsec: 50) at an accelerating voltage of 15 kV. To determine the average diameter of crystals in the enamel, 100 crystals were measured from an SEM image (for each fossilized sample) with the Fiji software. EDX was used to determine the contents of calcium (Ca), aluminum (Al), chlorine (Cl), iron (Fe), and silicon (Si) in the enamel. For studies on the local distribution of elements, EDX mapping of fossilized tooth samples containing dentin/cement and enamel was performed. The analysis was carried out in the enamel-dentin/cement-junction region for 15 h in the direction from the tooth interior (dentin/cement) towards the tooth surface (enamel).

Combustion analysis (Euro Vector, Euro EA elemental analyzer) was carried out to determine the contents of carbon (C), hydrogen (H), nitrogen (N), and sulfur (S). For further elemental analysis, 50 mg of sample was dissolved in ultrapure hydrochloric acid (37%, Fisher). The contents of calcium (Ca), sodium (Na), and magnesium (Mg) were determined by AAS (Thermo Electron, M-Series atomic absorption spectrometer). The content of phosphate (PO_4^{3-}) was determined by UV/VIS as phosphate-molybdenum blue complex (Agilent, Varian Cary 300 UV-Vis spectrophotometer). The content of fluorine (F) was determined by ISP (WTW, pH/ION 735), carried out by Analytische Laboratorien GmbH (Lindlar, Germany).

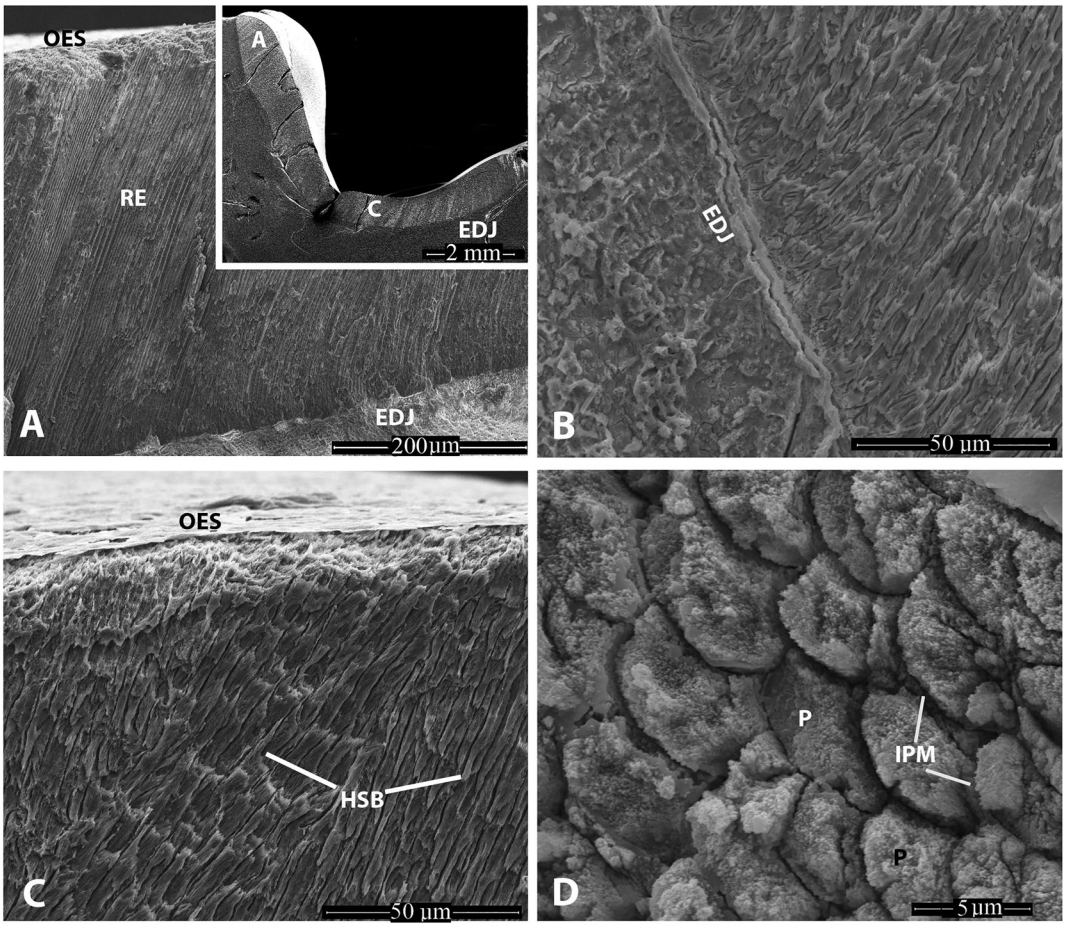

Figure 3. Scanning electron micrographs of enamel samples of *Moeritherium* (MO1) from late Eocene, Birket Qarun Formation, Fayum, Egypt. (a) Enlarged view of vertical section of upper molar fragment with areas close to the cusp apex (inset A) showing a schmelzmuster with radial enamel extending all the way up to the outer enamel surface (OES). (b) Enamel close to the base shows the presence of Hunter-Schreger bands (HSB) and prisms emerging at an angle to the enamel-dentine-junction (EDJ). (c) Enlarged view of vertical section close to the cusp base c in inset (a) Each HSB is around 10–15 prisms thick. (d) A tangential section cut slightly oblique to the prisms (P) shows a key-hole pattern surrounded by interprismatic matrix (IPM).

The contents of volatile water, organic compounds, and carbonated apatite were determined by TGA (Netzsch, STA 449 F3 Jupiter®). The measurements were performed in open alumina crucibles (containing 20 mg of sample), in a dynamic oxygen atmosphere, with a heating rate of 2 K min^{-1} in the temperature range of 30°C–1,400°C. The obtained TG data were processed with the Netzsch Proteus® software. The type of substitution in carbonated apatite was determined by IR spectroscopy (Bruker, Vertex 70). For IR analysis, the samples were prepared as potassium bromide (KBr) pellets with a diameter of 13 mm 2 mg of sample were ground with 200 mg of KBr (Sigma-Aldrich) and pressed under vacuum (Perkin-Elmer hydraulic press; KNF Neuberger vacuum pump) at a pressure of 5 t for 5 min to produce a transparent pellet. The measurements were performed from 400–4,000 cm^{-1}. The obtained IR data were processed with the Bruker Opus software.

XRD measurements were carried out to identify the crystalline phase of apatite and the possible diagenetic formation of other crystalline compounds in the fossilized teeth as well as to quantify the lattice parameters and crystallite size by Rietveld refinement. The small pieces of teeth parts were first pulverized to a fine powder and deposited on a flat silicon single crystal sample holder to minimize scattering after dispersing produced powder in ethanol for a better homogenization. All samples were investigated in Bragg-Brentano geometry in rotation mode with a Bruker D8 Advance instrument with CuKα radiation (1.54 Å, 40 kV and 40 mA). XRD analyses were performed for 5–90°2θ, step size 0.01°, counting time 0.6 s at each step, for a

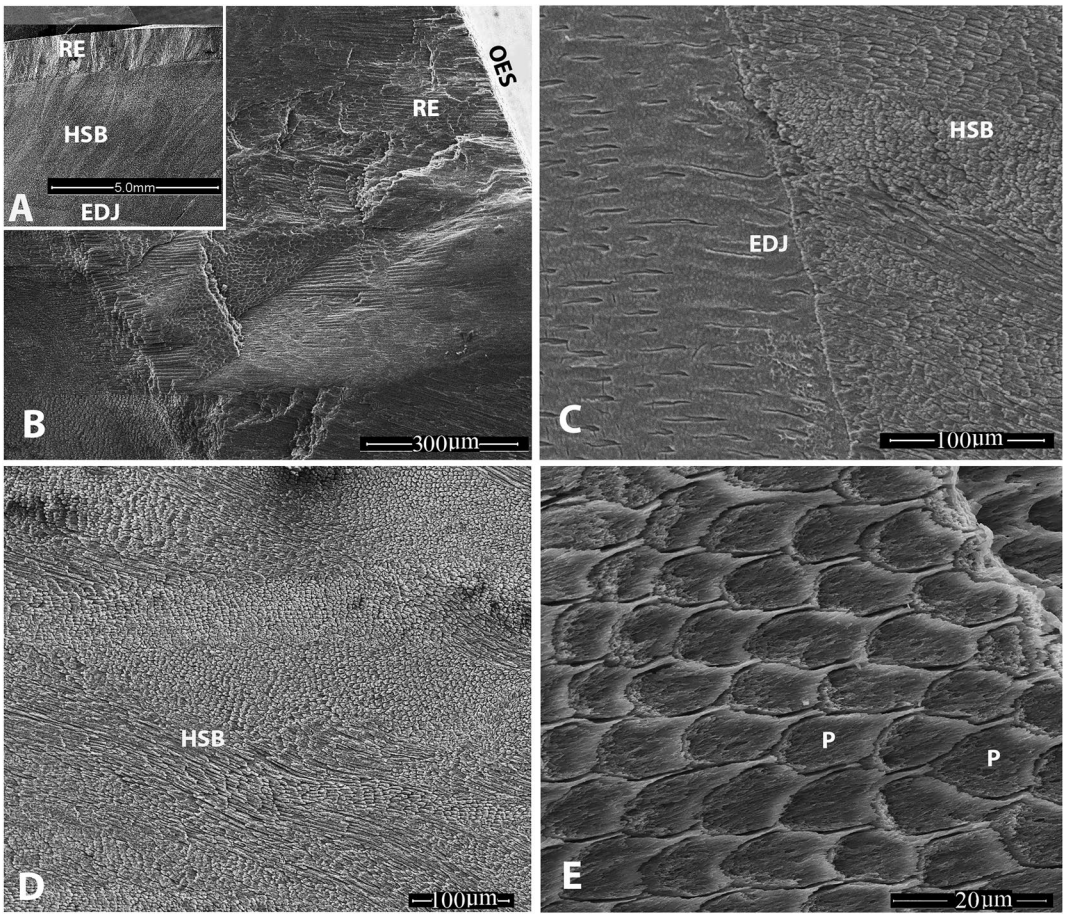

Figure 4. Scanning electron micrographs of enamel samples of *Palaeomastodon* (PAL) from late Eocene, Birket Qarun Formation, Fayum, Egypt. (a) and (b): Vertical section of a lower molar fragment showing an outer enamel schmelzmuster dominated by radial enamel. (c): Enamel close to the EDJ shows well developed HSB with prisms emerging out at an angle to the EDJ, including 3DE. (d): Irregular HSB with high degree of decussation. (e): A typical key-hole prism (P) pattern. EDJ, enamel-dentine-junction; HSB, Hunter-Schreger bands.

total measurement time of 90 min. The phase analysis was performed with the software Diffrac Suite EVA V1.2 from Bruker and reference patterns of fluorapatite FAP (#15–0876) from the ICDD database. For the determination of the lattice parameters *a*, *c*, and the crystallite size of hexagonal apatite, Rietveld refinement with the program package TOPAS 5.0 from Bruker was performed. The instrumental correction of the diffractometer parameters was done by measuring a standard powder sample (LaB_6; NIST; SRM 660b; $a = 4.15689$ Å).

To assess the extent of diagenetic alteration, we measured $\delta^{18}O$ of phosphate ($\delta^{18}O$-PO_4^{3-}) in tooth enamel from nine selected samples. The PO_4^{3-} in bioapatite was isolated as Ag_3PO_4 following the method reported by (Stephan, 2000) which is a slightly modified version of (O'Neil et al., 1994), at the Department of Geology, Panjab University, Chandigarh. 20 mg of powdered sample was extracted from each dental enamel sample with a Dremel drill. The powder was immersed in 2.5% aqueous NaOCl for 12 h to remove any soluble organic matter, followed by several times washing with distilled water. The washed sample was then immersed in 0.1 M aqueous NaOH for 48 h to remove any humic acid. After washing it several times with distilled water, the phosphate was dissolved in concentrated HF, and precipitated residual CaF_2 was removed by centrifugation. The solution was then neutralized with 2 M aqueous KOH, to which 15 ml of buffered silver diammine solution (0.2 M $AgNO_3$; 1.16 M NH_4NO_3; 0.75 ml concentrated NH_4OH) was added. The solution was heated to 60°C for several hours, resulting in precipitation of Ag_3PO_4, which was rinsed several times by distilled water, isolated by filtration, and dried in air. All chemicals used were of reagent grade. We have performed the NaOCl pretreatment during the isolation of phosphate from tooth

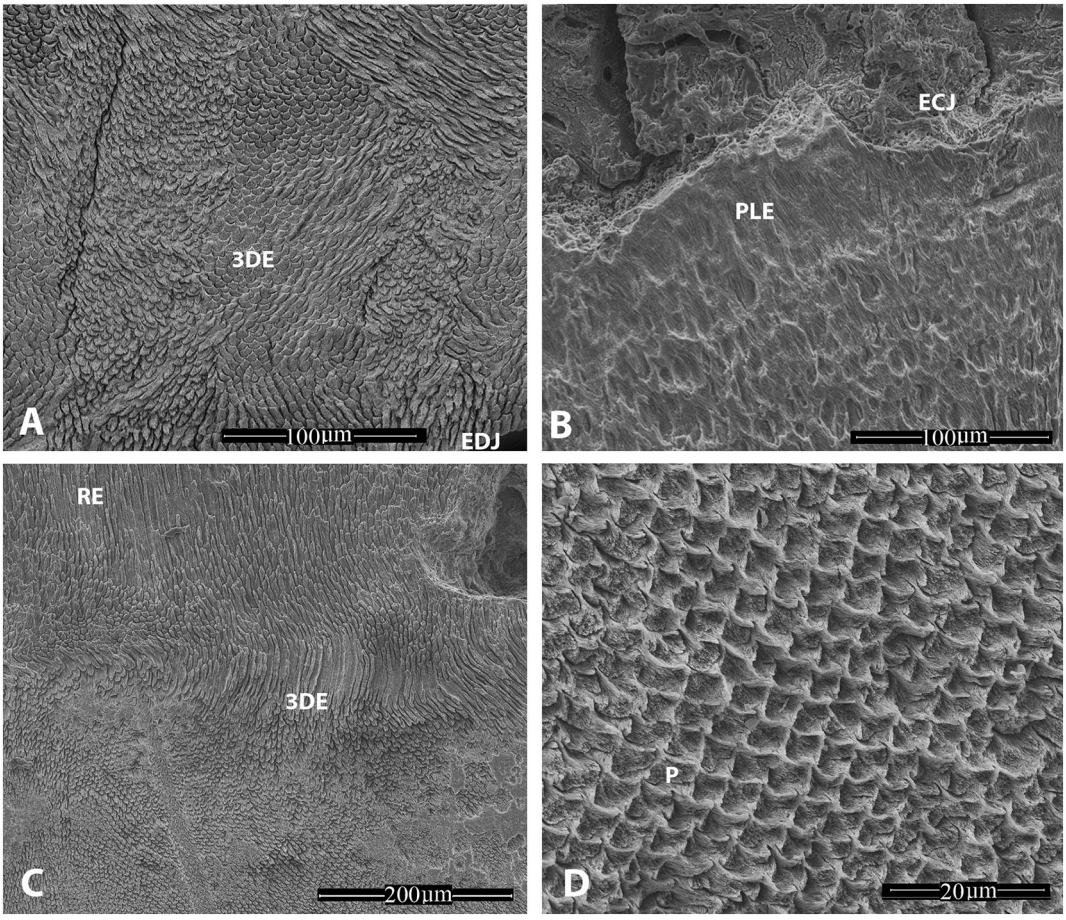

Figure 5. Scanning electron micrographs of enamel samples of *Palaeoloxodon namadicus* (PN) from Late Pleistocene (~50 Ka) Surajkund Formation, Hoshangabad (Madhya Pradesh, India). (a): Vertical section of the lower molar enamel showing 3DE close to the EDJ. (b): Prismless (PLE) enamel close to the ECJ (Enamel Cement Junction). (c): Central part with 3DE and upper part with RE. (d): Ginko-leaf prism (P) cross-section pattern surrounded by the IPM.

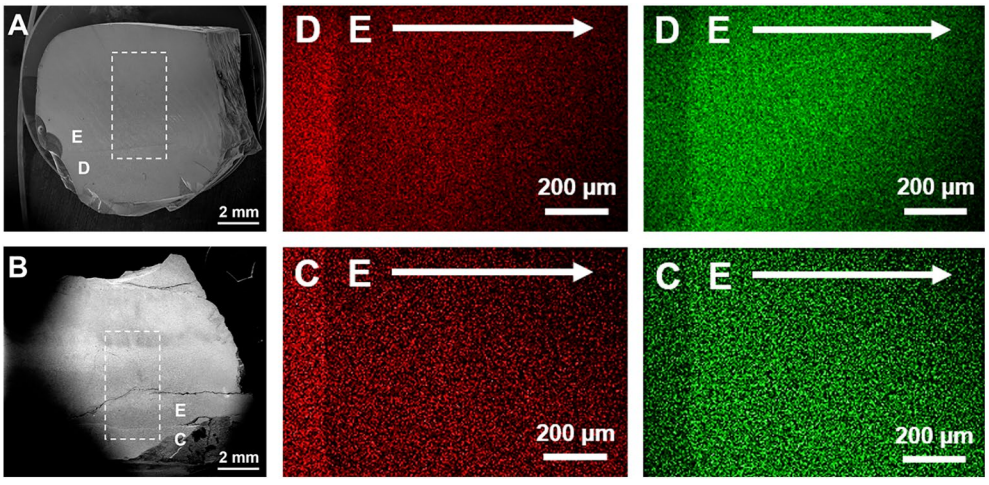

Figure 6. EDX elemental mapping of the dentin-enamel/dentin-cement junction of samples: AN: *Anancus* sp (A; 2.6–3 Ma) and SI: *Stegodon insignis* (B; 2.6–3 Ma). Scanning electron micrographs of the whole sample (gray) present the mapping region (marked with a white dashed line). Mapping of the local distribution of fluorine (red) and sodium (green) in the enamel. D dentin, C cement, E enamel. The fluoride content is higher in the dentin/cement, and the sodium content is higher in the enamel.

Table 2
All Characterization Data with Respect to the Chemical Composition of Enamel, Determined by Elemental Combustion Analysis (C, H, N, S), AAS (Ca, Na, Mg), ISP (F), UV/VIS (PO_4^{3-}), and EDX (Al, Cl, Fe, Si)

Sample	Ca/ wt%	PO_4^{3-}/ wt%	F/ wt%	Na/ wt%	Mg/ wt%	C/ wt%	H/ wt%	S/ wt%	N/ wt%	Al/ wt%	Cl/ wt%	Fe/ wt%	Si/ wt%	Ca/PO_4^{3-} molar ratio
MO1	35.3	47.9	1.47	0.62	0.11	1.51	0.45	<***	<***	0.79	<***	0.82	0.79	1.75 : 1
MO2	35.9	49.4	1.00	0.61	0.13	1.19	0.30	0.46	<***	0.50	0.33	0.93	0.86	1.72 : 1
PAL	36.6	50.7	0.95	0.78	0.15	1.71	0.45	<***	<***	0.16	<***	1.08	0.36	1.71 : 1
GO1	38.5	53.5	0.75	0.41	0.11	1.14	0.32	<***	<***	0.41	0.32	0.57	0.54	1.71 : 1
GO2	37.2	47.2	2.01	0.68	0.09	1.72	0.43	<***	<***	0.14	0.02	1.64	0.37	1.87 : 1
DE1	38.5	52.9	0.32	0.62	0.15	1.09	0.40	<***	<***	0.45	0.48	0.69	0.54	1.72 : 1
DE2	39.4	54.6	0.78	0.49	0.08	1.23	0.39	<***	<***	0.26	0.26	<***	0.43	1.71 : 1
AN	38.2	54.7	0.42	0.45	0.12	0.97	0.33	<***	<***	0.25	0.30	0.44	0.33	1.65 : 1
SI	39.1	54.4	0.40	0.55	0.13	1.07	0.34	<***	<***	0.08	0.15	<***	0.28	1.70 : 1
EP	38.2	51.5	0.97	0.57	0.10	1.63	0.41	<***	<***	0.24	0.14	0.44	0.52	1.76 : 1
EL	37.6	53.2	0.65	0.46	0.10	1.08	0.34	<***	<***	0.30	0.21	0.60	0.31	1.67 : 1
EH	38.2	50.7	0.92	0.54	0.12	1.72	0.45	<***	<***	0.34	0.31	0.69	0.47	1.79 : 1
PN	42.3	52.1	0.58	0.59	0.15	2.05	0.51	<***	<***	0.47	0.46	0.57	0.59	1.92 : 1
EM	37.0	51.4	0.04	0.63	0.24	1.48	0.41	<***	<***	0.41	<***	0.43	0.59	1.71 : 1

*** - Detection Limit.

enamel. However, it has been argued (Grimes & Pellegrini, 2013; Pederzani et al., 2020) that the 2.5% NaOCl pretreatment might lead to unexpected shifts in $\delta^{18}O\text{-}PO_4^{3-}$ of bioapatite and therefore should be avoided for samples with minor content of organic matter.

Table 3
The Crystallite Size and Diameter of Apatite Crystals Were Determined by XRD and SEM, Respectively. Apatite Substitution Type (B/A) and Ratio Were Determined by IR Spectroscopy, and the Carbonate Content in the Enamel was Determined by thermogravimetry.

Sample	Crystallite size (XRD)/nm	Diameter of crystals (SEM)/ nm	B/A substitution ratio	CO_3^{2-}/ wt%
MO1	52 ± 1	63 ± 14	2.0 : 1	2.0
MO2	39 ± 1	56 ± 10	3.0 : 1	1.4
PAL	39 ± 1	55 ± 10	2.5 : 1	0.7
GO1	35 ± 1	72 ± 12	2.5 : 1	1.4
GO2	24 ± 1	48 ± 9	2.5 : 1	3.4
DE1	24 ± 1	68 ± 11	2.5 : 1	1.4
DE2	32 ± 1	50 ± 11	3.0 : 1	1.4
AN	36 ± 1	43 ± 6	1.5 : 1	2.7
SI	44 ± 1	71 ± 12	3.0 : 1	2.0
EP	24 ± 1	48 ± 9	3.0 : 1	2.0
EL	38 ± 1	61 ± 11	3.0 : 1	2.0
EH	39 ± 1	58 ± 11	2.5 : 1	2.7
PN	37 ± 1	57 ± 10	3.0 : 1	2.0
EM	40 ± 1	56 ± 11	3.0 : 1	2.0

The oxygen in phosphate was converted quantitatively to CO by a standard pyrolysis method and subsequently its $^{18}O/^{16}O$ isotope ratio was determined. Analyses were performed with a TC/EA (High Temperature Conversion Elemental Analyzer) attached to an isotope ratio mass spectrometer (Delta V Plus IRMS, Thermo-Finnigan, Germany) in continuous flow mode at the West Australian Biogeochemistry Center. The detailed analytical protocol was described in (Halas et al., 2011). Normalization to the VSMOW scale was based on international reference materials provided by the International Atomic Energy Agency (IAEA-601: 23.3‰; IAEA-602: 71.4‰), following two-point normalization by (Paul et al., 2007), and verified by the phosphate rock standard NBS-120c ($\delta^{18}O_{VSMOW}$ = 21.7 ± 0.14‰) and a silver orthophosphate standard UMCS1 ($\delta^{18}O_{VSMOW}$ = 32.60 ± 0.12‰; see Halas et al., 2011). Isotope ratios are reported in the conventional δ-notation relative to VSMOW. The analytical uncertainty of $\delta^{18}O\text{-}PO_4^{3-}$ is < 0.5‰ (1 S.D.).

The $\delta^{18}O$ values (in the VPDB scale) of apatite carbonate presented in this study are taken from (Patnaik et al., 2019). Briefly, about 10 mg of tooth enamel powder was pretreated with NaOCl for 12 h and 1 M acetic acid for 6 h for organic matter removal, then centrifuged and rinsed in distilled water, freeze-dried for a maximum of 48 h. About 1–2 mg of treated samples were reacted with 100% H_3PO_4 in a Thermo-Finnigan Gasbench II peripheral device and the released CO_2 from the carbonate in the apatite was analyzed for $\delta^{18}O$ in continuous flow mode with a Thermo Scientific Delta V Plus Mass Spectrometer at the Indian Institute of Technology, Kanpur. Normalization to the VPDB scale was based on the international reference standards NBS19, L-SVEC, and CO-8, following

Table 4
Oxygen Isotope Ratios for Phosphate ($\delta^{18}O-PO_4^{3-}$) and Structural Carbonate ($\delta^{18}O-CO_3^{2-}$) in Tooth Enamel Apatite of Elephant and Rhinoceros

Sample name	Taxa	Age (Ma)	$\delta^{18}O-PO_4^{3-}$ (‰, VSMOW)	$\delta^{18}O-CO_3^{2-}$ (‰, VSMOW)	δCO_3-PO_4
EP	*Elephas platycephalus*	2.6–3.0	14.5	26.0	11.6
PN	*Palaeoloxodon namadicus*	0.05	17.3	31.0	13.7
A155	*Elephas planifrons*	1.5–2.5	14.1	23.8	9.8
VPL/B 2060	*Elephas hysudricus*	0.5	11.9	24.6	12.7
EL	*Elephas hysudricus*	1.5	14.3	25.2	11.0
RB41	Rhinocerotidae	13–14	7.3	17.8	10.5
DD1	*Deinotherium* sp.	11	8.9	22.0	13.1
B608	*Elephas planifrons*	2.6–3.0	10.9	25.1	14.2
GO1	Gomphotheridae	13–14	7.1	20.2	13.1

multi-point normalization (Paul et al., 2007). The analytical uncertainty of $\delta^{18}O$-CO_3^{2-}, based on repeated analysis of Carrara Marble standard ($\delta^{18}O_{VPDB} = -2.01$) was 0.11‰ (1 S.D.). The $\delta^{18}O$-CO_3^{2-} values in VPDB scale were converted to VSMOW scale using the equation suggested by Coplen et al.: $\delta^{18}O_{VSMOW} = 1.03091\ \delta^{18}O_{VPDB} + 30.91$ (Coplen, 1988).

3. Results and Discussion

We performed a comprehensive study on the elemental composition and microstructure of fossilized enamel of 13 different extinct elephants (Table 1) as well as of the enamel of a recent elephant as reference. We also undertook stable oxygen isotope studies on nine proboscidean and one rhinoceratid dental enamel samples from the same Neogene-Quaternary sites as studied for elemental composition and microstructure. Figure 1 gives a timeline on the origin of the elephants, and Figure 2 shows a map of fossil locations.

All enamel samples showed a well-preserved enamel microstructure, even in the oldest samples. The applied process of sample preparation for SEM imaging, in particular diamond polishing and nitric acid etching steps, does not significantly alter the prismatic and interprismatic crystal microstructure of the enamel as shown before (Puech et al., 1986; Risnes & Li, 2019).

We describe here, for the first time from India, the enamel microstructure of extant and fossil elephantiforms such as *Elephas maximus*, *Elephas platycephalus*, *Palaeoloxodon namadicus*, *Anancus*, and *Stegodon*. For comparison we have studied some of the early proboscideans such as *Moeritherium* and *Palaeomastodon* from Egypt. *Moeritherium* (MO1 and MO2) enamel fragments were collected from late Eocene, Birket Qarun Formation, Fayum, Egypt. Additional SEM images can be found in the Supporting Information.

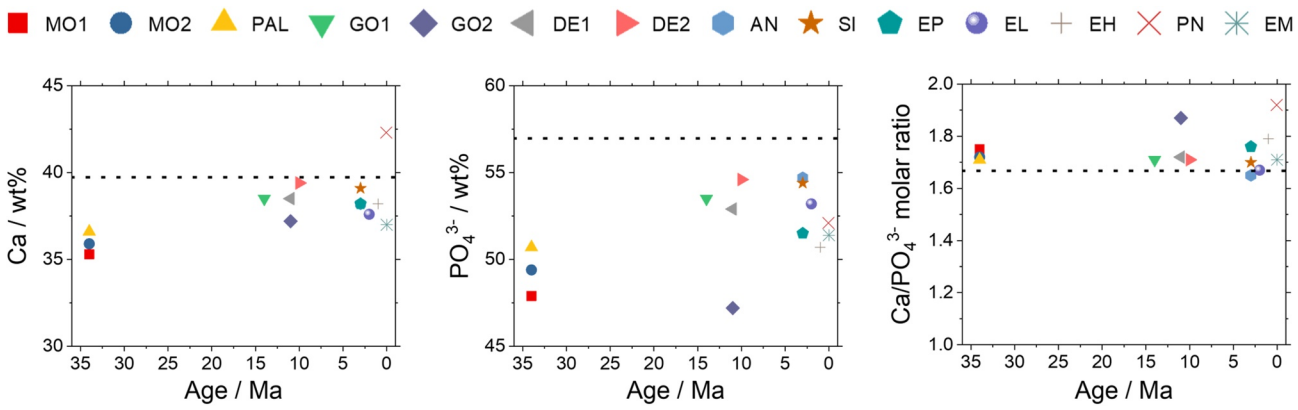

Figure 7. A summary of calcium (Ca^{2+}, left) and phosphate (PO_4^{3-}, center) content in the enamel samples. The theoretical contents of calcium and phosphate in pure hydroxyapatite are 39.9 wt% and 56.7 wt%, respectively (dashed line). Based on these results, the Ca/PO_4^{3-} molar ratio in bioapatite in the enamel samples was determined (right). The theoretical Ca/PO_4^{3-} molar ratio in pure hydroxyapatite is 1.67 (dashed line).

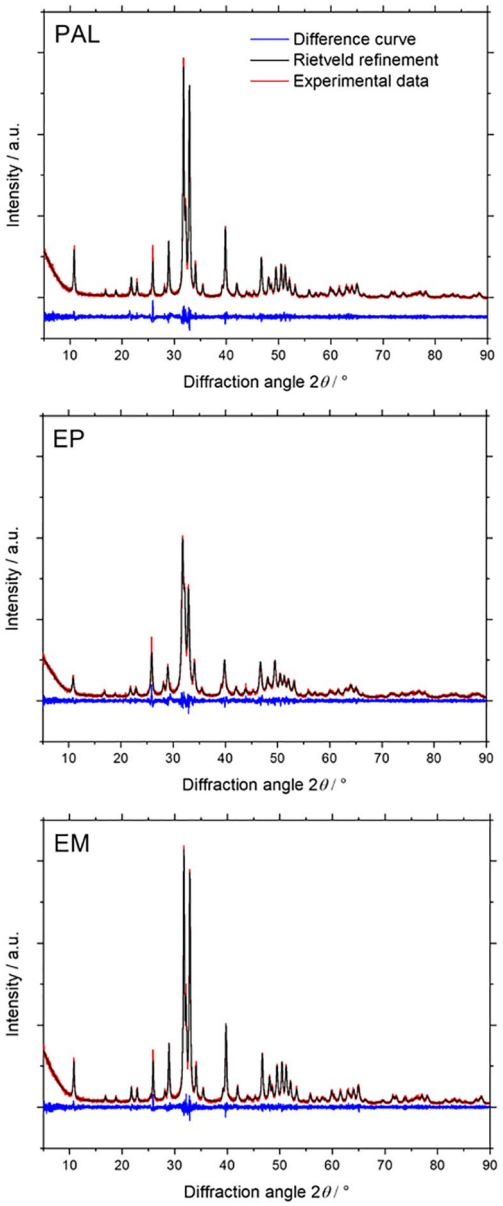

Figure 8. Representative XRD powder diffractograms of the enamel of samples PAL: *Palaeomastodon* (34 Ma), EP: *Elephas platycephalus* (2.6–3 Ma), and EM: *Elephas maximus* (recent), including Rietveld refinement with the hydroxyapatite structure.

A vertical section of the upper molar fragment of MO1 showed a two-layered schmelzmuster comprising thin HSBs developed close to tooth basin, whereas the apex portion was made mostly of RE. The prisms showed the primitive key-hole pattern (Figure 3). Earlier studies on *Moeritherium* from Egypt (Bertrand, 1988; Pfretzschner, 1994) and Algeria (Tabuce et al., 2007) also showed the presence of the thin HSBs (a primitive character) and RE, with a key-hole prism pattern exposed in a tangentially cut cross-section.

Palaeomastodon (PAL) enamel fragments were collected from the late Eocene, Birket Qarun Formation, Fayum, Egypt. A vertical section of the lower molar fragment showed two layered (HSB and RE) schmelzmuster. The outer enamel layer was made up of RE, whereas HSB occupied the inner part of the enamel (Figure 4). Prisms showed a primitive key-hole pattern. *Palaeomastodon*, therefore, shows a primitive schmelzmuster and prism pattern similar to that of *Moeritherium* (Bertrand, 1988; Kozawa, 1978).

Deinotherium (DE1) from Late Miocene (10–11 Ma), deposits of Kutch (Gujarat, India), showed a 3-layered (3DE, HSB, and RE) schmelzmuster and a fan-shaped prism cross-section pattern (Figure S4). Earlier studies on *Deinotherium* by (Bertrand, 1988) and (Pfretzschner, 1994) showed the presence of 3DE and key-hole prism cross-section patterns. (Patnaik et al., 2014) studied *Deinotherium* from Late Miocene of Kutch and found HSB, 3DE and RE schmelzmuster and a key-hole prism pattern in their microstructure.

Gomphotherium (GO1) enamel fragments collected from Middle Miocene Siwalik deposits exposed around Ramnagar (Jammu and Kashmir, India) belong to the Chinji Formation (~14–13 Ma). The enamel was very thick and in vertical sections showed a schmelzmuster consisting of 3DE, HSB, and RE and a typical fan-shaped prism cross-section pattern (Figure S5). Earlier studies on *Gomphotherium*/Gomphotheridae enamel gave similar results, that is, the presence of 3DE, HSB, and RE, and also a fan-shaped prism cross-section (Bertrand, 1988; Patnaik et al., 2014).

A lower molar of *Anancus* (AN) was collected from Late Pliocene (2.6–3 Ma) Siwalik sediments belonging to the Tatrot Formation exposed around Khetpurali (Haryana, India). A vertical section of the lower molar enamel showed a 3-layered (3DE, HSB, and RE) schmelzmuster. 3DE formed very close to the EDJ, whereas a major part of the inner enamel was dominated by HSB of variable thickness. RE was thick lying above the HSB layer and close to OES (Figure S6). The prism cross-section pattern was fan-shaped. An earlier study of *Anancus* enamel microstructure from Lower Pliocene deposits of Tuscany, Italy showed similar 3DE, HSB, and RE schmelzmuster and a fan-shaped prism pattern (Ferretti, 2007).

A *Stegodon insignis* lower molar (SI) was collected from Late Pliocene (2.6–3 Ma) Siwalik deposits belonging to the Tatrot Formation outcropping around the Village Nathunala (Punjab, India). Its vertical section clearly showed the presence of 3DE close to the EDJ (SI Figure S7). The part of the enamel often consists of HSB followed by RE close to the OES. In some areas, prismless (PLE) enamel close to OES was also seen. The prism (P) cross-section pattern was of the ginko-leaf type. (Ferretti, 2007) studied the enamel of *Stegodon* collected from Pleistocene sediments of Sangiran, Java, and also found a similar 3-layered (3DE, HSB, and RE) schmelzmuster and ginko-leaf prism pattern.

An *Elephas platycephalus* (EP) skull with upper molars was collected from Upper Siwaliks (Tatrot Formation) Late Pliocene (2.6–3 Ma), from Quranwala (Punjab, India). The vertical section of the upper mo-

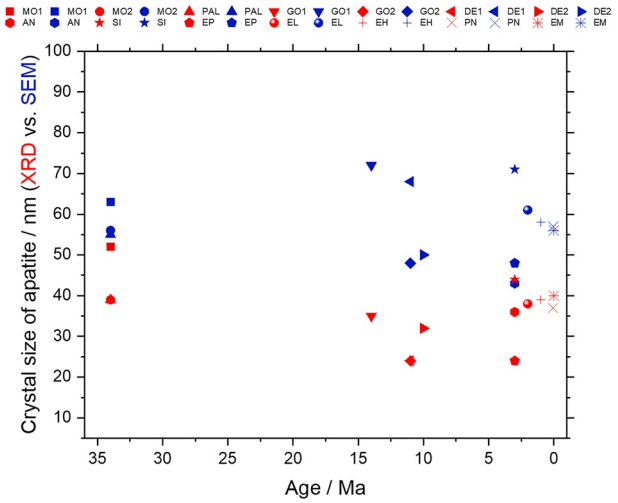

Figure 9. Comparison of the results of crystallite size and crystal diameter in bioapatite in enamel studied by XRD (red) and SEM (blue).

lar enamel clearly showed the development of 3DE close to the EDJ (SI Figure S8). Beside HSB and RE, prismless (PLE) enamel close to the ECJ (Enamel Cement Junction) was also observed. A ginko-leaf prism (P) cross-section pattern was present. (Ferretti, 2007) studied the modern Asian elephant enamel of *Elephas maximus* and observed the presence of 3-layered (3DE, HSB, and RE) schmelzmuster and ginko-leaf prism pattern. We have also studied *Elephas maximus* (EM) enamel and found a very similar pattern in addition to the presence of PLE close to the ECJ (see Supporting Information).

Palaeoloxodon namadicus (PN) upper molar enamel was extracted from a skull collected from the Late Pleistocene (~50 Ka) Surajkund Formation, Hoshangabad (Madhya Pradesh, India), in a very well-preserved condition. 3DE was very well-developed and occupied most of the enamel area starting from the EDJ. Towards the enamel cement junction, the 3DE gave rise to RE, which in turn developed into PLE. The prism pattern was the advanced ginko-leaf type as seen in *Elephas* and *Stegodon*. The prisms were surrounded by well-defined jacket (evident due to differential etching) formed by the IPM (Figure 5).

Overall, the enamel microstructure of the proboscideans studied here ranging in age from Late Eocene to Late Pleistocene was well-preserved. Phylogenetically, the African taxa of *Moeritherium* and *Palaeomastodon* with low-crowned teeth showed a primitive schmelzmuster condition with HSB and RE, and also a primitive prism cross-section pattern of key-hole type. We have observed 3DE, HSB, and RE in the lophodont *Deinotherium* which confirms the presence of this type of schmelzmuster reported earlier (Patnaik et al., 2014), contrary to the findings of (Bertrand, 1988) and (Pfretzschner, 1994) who observed only 3DE in them. This study also confirms the earlier findings of bunodont thick enameled *Gomphotherium*/Gomphotheridae and *Anancus* having an enamel microstructure with 3DE, HSB, and RE and fan-shaped prism cross-section (Bertrand, 1988; Ferretti, 2007; Patnaik et al., 2014). The brachydont *Stegodon* showed the presence of PLE beside 3DE, HSB, and RE; it also showed, at some places, the primitive pattern 1 prism cross-section beside the advanced ginko-leaf pattern. The hypsodont *Elephas* and *Palaeoloxodon* enamel was dominated by 3DE, but at places, HSBs were seen where the enamel became thinner. Both taxa showed the development of extensive PLE close to the ECJ and ginko-leaf prism cross-section pattern.

3.1. Elemental Analyses

A local elemental analysis of the EDJ/ECJ is shown in Figure 6 for two representative samples. Within the teeth, differences between dentin/cement and enamel in the local distribution of elements were observed. A higher content of fluorine was found in the dentin/cement, whereas sodium was more abundant in the enamel. The farther from the EDJ/ECJ, the less fluorine was found. This observation is consistent with earlier reports (Wilmers & Bargmann, 2020). Unfortunately, for our results, no data concerning proboscideans were available for comparison, but a similar fluorine distribution tendency has been reported in non-fossilized human teeth (Nakagaki et al., 1987). Furthermore, Dauphin and Williams reported that fossilized enamel of various mammals (e.g., Pleistocene rats) was sodium-enriched in comparison to dentin (Dauphin & Williams, 2007, 2008).

Figure 7 shows the calcium and phosphate content in the enamel of all samples from elemental analysis by AAS and UV/VIS, respectively. This can be converted into the molar calcium-to-phosphate ratio, which is an indication of the calcium phosphate phase present. All data are comprised in Table 2. The contents of calcium and phosphate in proboscidean enamel apatite were stable over time, without significant differences found between the oldest and the youngest samples. Similar observations were reported for shark enamel (Kocsis et al., 2014; Luebke et al., 2015, 2017). Generally, the contents of calcium and phosphate in fossilized proboscidean enamel were close to the theoretical values in pure hydroxyapatite, but the lower values, particularly for phosphate, indicate ionic substitutions of enamel apatite (bioapatite). These may be Mg^{2+} for Ca^{2+}, F^{-}/CO_3^{2-} for OH^{-} and HPO_4^{2-}/CO_3^{2-} for PO_4^{3-} (Sakae et al., 1991). A similar age-dependence of the Ca/P ratio in fossilized and modern mammalian enamel was reported by (Roche et al., 2010). The elemental analysis data of the light elements (C, H, S, and N) are given in Table 2. It confirms the low organic content

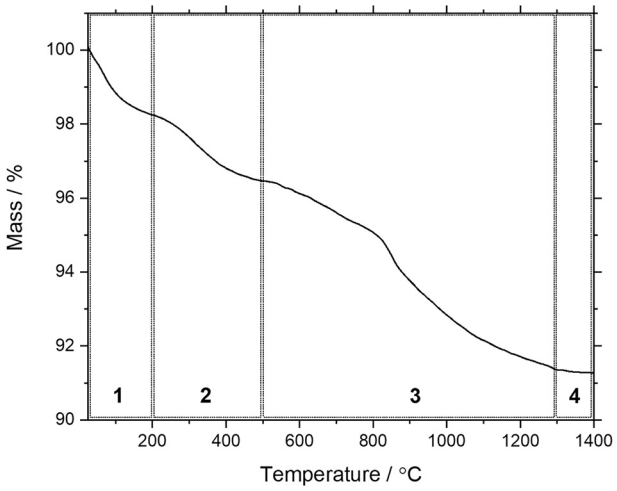

Figure 10. Representative thermogram of the enamel of sample EP: *Elephas platycephalus*; (2.6–3 Ma). Region 1: Release of adsorbed water. Region 2: Combustion of organic material and release of structural water. Region 3: Release of CO_2 from carbonated apatite (bioapatite). Region 4: Remaining pure inorganic material (apatite).

in the fossilized teeth, that is, about 1 wt%–2 wt% C and 0.3 wt%–0.5 wt% H. This agrees well with the results from thermogravimetry (see below).

The crystalline phase in the enamel was analyzed by X-ray powder diffraction on ground samples (Figure 8). Enamel showed a common XRD pattern for proboscideans, showing nanocrystalline apatite as indicated by the broad diffraction peaks from which the crystallite size can be derived (smaller crystallites give broader diffraction peaks) (Klug & Alexander, 1974). A detailed Rietveld refinement gave the crystallite size. Furthermore, XRD results showed changes in the apatite lattice parameters (mostly an increase of the *a*-axis length) which indicates an ionic substitution of enamel apatite (bioapatite) and therefore confirmed our interpretation of the AAS results.

The crystallite sizes from X-ray diffraction can then be compared with the particle size obtained by SEM (Figure 9). Neither for crystallite size (by XRD) nor for crystal size (by SEM), a significant change with age was found. Differences between the crystallite/crystal size values between the above methods can be explained by the peculiarities of the methods that probe different sample properties. XRD determines crystallite sizes (technically the diameter of coherently scattering crystalline domains in a crystal) which are usually smaller than total particle diameter. Thus, each particle (by SEM) may consist of more than one crystallite (by XRD), i.e. it is usually not a single crystal. Therefore, the particle size is by SEM is generally higher than the crystallite size by XRD. Typically, the apatite crystals were 30–40 nm and 40–70 nm in size by XRD and SEM, respectively (Table 3). No other crystalline phases that might have been related to diagenesis were found by XRD.

In a comparable study (Sakae et al., 1991),investigated fossilized enamel of proboscideans by XRD covering the age range from Eocene to Pleistocene and reported a common XRD pattern of proboscidean enamel, which was also similar to the XRD pattern of human enamel. (Bracco et al., 2013) reported that recent ivory and mammoth teeth contain mainly bioapatite with low crystallinity.

Thermogravimetry gives further information on the enamel composition (Figure 10). All studied samples had a similar TG pattern with an average mass loss of ~10%. Based on the TGA results, the content of carbonate in enamel apatite was calculated (Peters et al., 2000). The carbonate content of about 2 wt% by TGA (Table 3) was lower than the carbonate amount typically found in bioapatite of recent teeth (3 wt%–7 wt%) (Dorozhkin & Epple, 2002; Elliott, 2002; Enax et al., 2013) but in the range found for fossilized shark teeth (about 2 wt% as average for enamel and dentin) (Enax et al., 2012). However, it is unclear due to the small sample size whether this really indicates an effect of fossilization. A significant correlation between the age of the sample and the carbonate content was not found.

Infrared spectroscopy gives insights into the substitution of carbonate in the apatite lattice (Figure 11). In all IR spectra of the studied samples we found a B-type substitution of carbonated apatite (CO_3^{2-} on PO_4^{3-} positions) as preferential to A-type substitution (CO_3^{2-} on OH^- positions) (Nowicki et al., 2018).

The fluoride content in the fossilized enamel was significantly higher than in the recent sample (Table 2). This agrees with the report of Roche et al. who investigated fossilized tooth enamel of different Miocene-Pliocene mammalian taxa, including proboscideans (Roche et al., 2010). We did not observe a significant age-dependency of the fluoride content in the enamel among the fossils. Our results confirm the general assumption that there is no clear relationship between fluoride content and the time of fossilization (Roche et al., 2010; Sakae et al., 1991). Puech et al. observed that the fluoride content in fossilized fish teeth was species-related and not influenced by the environmental fluoride (Puech et al., 1986). No clear age-relationship was found for the contents of magnesium, sodium, carbon, hydrogen, and chlorine. Moreover, no significant differences in the contents of Si, Fe, and Al (elements of diagenetic origin) were found, among fossils of different ages, which indicates a considerable resistance of enamel to chemical alteration or diagenesis during fossilization.

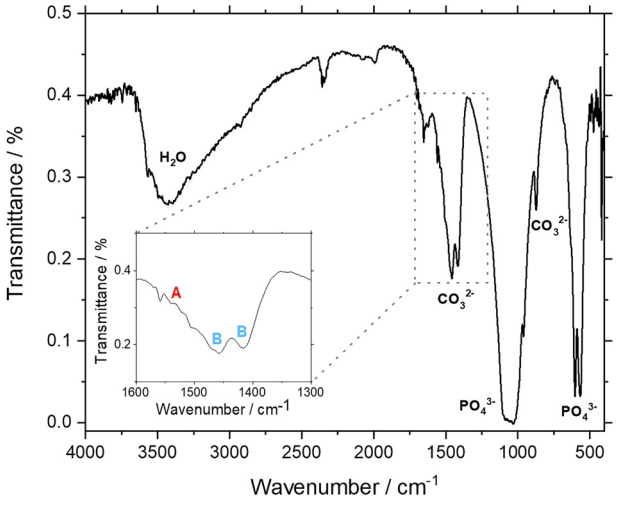

Figure 11. Representative IR spectrum of the enamel of sample DE2: *Deinotherium* sp (9–10 Ma). The region 1,300–1,600 cm^{-1} (labeled with a dashed line) shows the type of substitution (A/B type) in carbonated apatite (Fleet, 2017; Fleet et al., 2004; Garskaite et al., 2014).

Because the strength of a C—O bond is less than that of a P—O bond, the oxygen isotopic composition of CO_3^{2-} ($\delta^{18}O\text{-}CO_3^{2-}$) is more likely to be affected by diagenesis than the $\delta^{18}O\text{-}PO_4^{3-}$ of hydroxyapatite (Lee-Thorp & van der Merwe, 1991). The relationship between $\delta^{18}O$ of PO_4^{3-} and CO_3^{2-} of enamel apatite has been used as a diagnostic tool to determine the effect of diagenetic alteration on the preservation of primary isotopic composition (Zazzo, Lécuyer, Sheppard, et al., 2004). Studies have shown that the $\delta^{18}O\text{-}PO_4^{3-}$ value (‰, VSMOW) is typically ~9‰ less than the $\delta^{18}O\text{-}CO_3^{2-}$ value (‰, VSMOW) ($\alpha_{CO3\text{-}PO4}$ = 1.0086 ± 0.0007; (Bryant et al., 1996); and $\alpha_{CO3\text{-}PO4}$ = 1.0089 ± 0.0007; (Iacumin et al., 1996); see also (Longinelli & Nuti, 1973; Miller et al., 2018). Generally, a $\Delta_{CO3\text{-}PO4}$ of ~9%, also reported at an intra-tooth level, indicates a good preservation of the primary isotopic signature in fossil apatite (Martin et al., 2008) and references therein). Once the primary nature of isotopic composition is ascertained, then the oxygen isotopic composition of carbonate or phosphate fraction of enamel apatite can be used to obtain the $\delta^{18}O$ of body water of mammals and by extension the $\delta^{18}O$ of local environmental water that also reflects the nature of meteoric precipitation (e.g., Ayliffe et al., 1994, 1992; Iacumin et al., 1996; Miller et al., 2018; Zazzo, Lécuyer, Sheppard, et al., 2004).

The $\Delta_{CO3\text{-}PO4}$ in our samples varied within a range of 10%–14% (Table 4). Figure 12 shows only two fossil tooth apatite samples lying close to the equilibrium line established for modern mammals, deers, and carbonate shells (Bryant et al., 1996; Iacumin et al., 1996; Miller et al., 2018), which indicates that most of our samples experienced some extent of diagenetic alteration. However, no correlation was observed between the extent of alteration and the age of the sample. The implication of this result is that whereas the $\delta^{18}O\text{-}PO_4^{3-}$ of tooth enamel of the analyzed samples can still be used as a more reliable proxy for body water of mammals (and in turn for environmental/meteoric water (Ayliffe et al., 1994, 1992; Zazzo, Lécuyer, & Mariotti, 2004), the $\delta^{18}O\text{-}CO_3^{2-}$ values in these enamels should be carefully considered for paleoclimate reconstruction because as stated earlier these ratios in the carbonate fraction are more susceptible to diagenetic alteration. Interestingly, two of our samples GO1 and RB41 (Mid-Miocene age) had the lowest $\delta^{18}O\text{-}PO_4^{3-}$ values of about 7‰ (Table 4) which would translate to $\delta^{18}O$ of ingested water (assumed to be same as precipitation) of about −15%, using the equation 1b of (Ayliffe et al., 1992) that relates the $\delta^{18}O\text{-}PO_4^{3-}$ of bone and teeth of modern elephants with $\delta^{18}O$ of ingested water, and considers the associated uncertainties in the slope and intercept. The sample RB41 lies very close to the equilibrium line, indicating a good preservation (Figure 12). Because enamel microstructure and elemental composition obtained from other methods (XRD, SEM, UV/VIS, IR, TG) indicate a good preservation of our fossilized teeth samples, the isotopic composition of these two Mid-Miocene samples suggest the possibility that these two animals could have migrated from farther north, possibly from higher elevations in the Himalayas as characterized by ^{18}O-depleted precipitation.

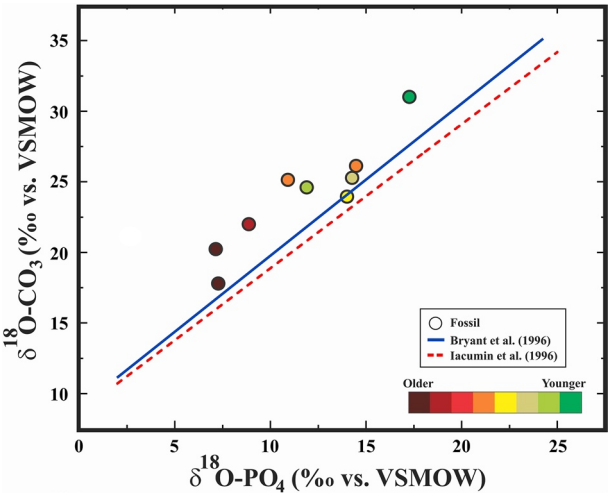

Figure 12. $\delta^{18}O$ of coexisting PO_4^{3-} and CO_3^{2-} in biogenic apatite in dental enamel from eight proboscidean and a rhinoceratid samples of Neogene-Quaternary age (Table 4). The solid line represents equilibrium lines proposed by these two co-existing phases determined for recent mammals (Bryant et al., 1996; Iacumin et al., 1996). Data from (Longinelli & Nuti, 1973), based on recent carbonate shells, (Miller et al., 2018), based on recent deer tooth enamel, and (Martin et al., 2008), based on recent rhinoceros enamel, also lie near the two equilibrium lines obtained for modern mammals.

4. Conclusions

We studied fossilized enamel of different proboscideans. The fossilized samples covering a time range from late Eocene (~34 Ma) to late Pleistocene (~0.05 Ma), and were recovered from various locations in Egypt and India. Enamel of a recent Asian elephant (*E. maximus*) was used as reference. The distinct prismatic microstructure of the enamel was well-preserved, independent of the age of the samples. Our results support the earlier findings that the African taxa of *Moeritherium* and

Palaeomastodon show primitive schmelzmuster condition (HSB and RE) and key-hole prism cross-section pattern. We here presented for the first time enamel microstructure data of Indian *Anancus*, *Stegodon*, *Elephas*, and *Palaeoloxodon*. We observed the widespread occurrence of PLE in *Stegodon*, *Elephas*, and *Palaeoloxodon* and pattern 1 prism cross-section in *Stegodon* beside the ginko-leaf pattern. The contents of calcium and phosphate in bioapatite were similar in all samples studied and close to stoichiometric hydroxyapatite. In fossilized samples, an increased content of fluoride was observed in comparison to the recent sample, however without a clear age-dependency. The obtained data confirmed the presence of ionic substitutions in enamel apatite, its purity, and its nanocrystalline nature. Enamel had a low content of carbonate, and a B-type substitution of carbonated apatite was found to be preferential (carbonate on phosphate positions). Small amounts of externally incorporated elements from diagenesis, that is, Si, Al, and Fe were found in the enamel. However, a lack of age-dependency within the Siwaliks of the Himalayan Foreland Basin indicates that diagenesis had no significant influence on the studied samples. Furthermore, we report the first results on the depth-related local distribution of elements (Na, F) in the teeth of extinct proboscideans. The oxygen isotope composition of phosphate and carbonate in enamel apatite indicate minor to moderate modifications of the isotopic ratios of enamel carbonate due to the diagenetic alteration of most of the samples. Nevertheless, its chemical stability and the high resistance to microstructure alterations during diagenesis gives enamel an advantage over dentin and bone and makes it an excellent material for chemical and paleontological studies on extinct taxa, which can be used as proxy for paleoclimate and their paleoenvironment.

Data Availability Statement

All data from this study can be accessed from zenodo (https://doi.org/10.5281/zenodo.4646219) as well as in the supporting information files with this article.

Acknowledgments
Matthias Epple and Rajeev Patnaik thank the Department of Science and Technology (DST) and Deutscher Akademischer Austauschdienst (DAAD) for funding this project. The authors also thank Tobias Bochmann and Smail Boukercha for SEM imaging, and Robin Meya for AAS analyses. Rajeev Patnaik was supported by MoES/P.O. (Geosci)/46/2015 and SERB-HRR/2018/000063 for field work in the Siwaliks, Narmada Valley, and Kutch, and isotope analysis. We are grateful to Kateryna Loza and Ankita Singla for conducting preliminary analyses and for experimental assistance.

References

Abbas, S. G., Khan, M. A., Babar, M. A., & Akhtar, M. (2019). New remains of Elephantidae from the Upper Siwalik subgroup (Plio-Pleistocene) of Pakistan. *Quaternary Science Reviews*, *224*, 105967. https://doi.org/10.1016/j.quascirev.2019.105967

Abbas, S. G., Khan, M. A., Babar, M. A., Hanif, M., & Akhtar, M. J. (2018). New materials of Choerolophodon (Proboscidea) from Dhok Pathan Formation of Siwaliks, Pakistan. *Vertebrata PalAsiatica*, *56*, 295–305. https://doi.org/10.19615/j.cnki.1000-3118.180103

Ayliffe, L. K., Chivas, A. R., & Leakey, M. G. (1994). The retention of primary oxygen isotope compositions of fossil elephant skeletal phosphate. *Geochimica et Cosmochimica Acta*, *58*(23), 5291–5298. https://doi.org/10.1016/0016-7037(94)90312-3

Ayliffe, L. K., Lister, A. M., & Chivas, A. R. (1992). The preservation of glacial-interglacial climatic signatures in the oxygen isotopes of elephant skeletal phosphate. *Palaeogeography, Palaeoclimatology, Palaeoecology*, *99*(3–4), 179–191. https://doi.org/10.1016/0031-0182(92)90014-v

Ben-Zvi, Y., Maria, R., Pierantoni, M., Brumfeld, V., Shahar, R., & Weiner, S. (2019). Response of the tooth-periodontal ligament-bone complex to load: A microCT study of the minipig molar. *Journal of Structural Biology*, *205*, 155–162. https://doi.org/10.1016/j.jsb.2019.01.002

Bertrand, P. (1988). Évolution de la structure de l'émail chez les Proboscidea primitifs: Aspects phylogénétique et fonctionnel. In D. E. Russell, J. P. Santoro, & D. Sigogneau-Russell (Eds.), Teeth revisited: Proceedings of the 7th international symposium on dental morphology (53 pp. 109–124). Mémoires du Museum national d'histoire naturelle Série C Géologie.

Boyde, A. (1967). The development of enamel structure. *Proceedings of the Royal Society of Medicine*, *60*, 923–928. https://doi.org/10.1177/003591576706000965

Bracco, S., Brajkovic, A., Comotti, A., & Rolandi, V. (2013). Characterization of elephant and mammoth ivory by solid state NMR. *Periodico di Mineralogia*, *82*, 239–250. https://doi.org/10.2451/2013PM0014

Bryant, J. D., Koch, P. L., Froelich, P. N., Showers, W. J., & Genna, B. J. (1996). Oxygen isotope partitioning between phosphate and carbonate in mammalian apatite. *Geochimica et Cosmochimica Acta*, *60*, 5145–5148. https://doi.org/10.1016/S0016-7037(96)00308-0

Coplen, T. B. (1988). Normalization of oxygen and hydrogen isotope data. *Chemical Geology: Isotope Geoscience Section*, *72*, 293–297. https://doi.org/10.1016/0168-9622(88)90042-5

Daculsi, G., & Kerebel, L. M. (1980). Ultrastructural study and comparative analysis of fluoride content of enameloid in sea-water and fresh-water sharks. *Archives of Oral Biology*, *25*, 145–151. https://doi.org/10.1016/0003-9969(80)90013-8

Daculsi, G., LeGeros, R. Z., Heughebaert, M., & Barbieux, I. (1990). Formation of carbonate-apatite crystals after implantation of calcium phosphate ceramics. *Calcified Tissue International*, *46*, 20–27. https://doi.org/10.1007/bf02555820

Dauphin, Y., & Williams, C. T. (2007). The chemical compositions of dentine and enamel from recent reptile and mammal teeth-variability in the diagenetic changes of fossil teeth. *CrystEngComm*, *9*, 1252–1261. https://doi.org/10.1039/b708985f

Dauphin, Y., & Williams, C. T. (2008). Chemical composition of enamel and dentine in modern reptile teeth. *Mineralogical Magazine*, *72*, 247–250. https://doi.org/10.1180/minmag.2008.072.1.247

Dorozhkin, S. V., & Epple, M. (2002). Biological and medical significance of calcium phosphates. *Angewandte Chemie International Edition*, *41*, 3130–3146. https://doi.org/10.1002/1521-3773(20020902)41:17<3130::aid-anie3130>3.0.co;2-1

Eder, M., Amini, S., & Fratzl, P. (2018). Biological composites-complex structures for functional diversity. *Science*, *362*, 543–547. https://doi.org/10.1126/science.aat8297

Elliott, J. C. (2002). Calcium phosphate biominerals. *Reviews in Mineralogy and Geochemistry*, *48*, 427–453. https://doi.org/10.2138/rmg.2002.48.11

Enax, J., Fabritius, H.-O., Rack, A., Prymak, O., Raabe, D., & Epple, M. (2013). Characterization of crocodile teeth: Correlation of composition, microstructure, and hardness. *Journal of Structural Biology*, *184*, 155–163. https://doi.org/10.1016/j.jsb.2013.09.018

Enax, J., Prymak, O., Raabe, D., & Epple, M. (2012). Structure, composition, and mechanical properties of shark teeth. *Journal of Structural Biology*, *178*, 290–299. https://doi.org/10.1016/j.jsb.2012.03.012
Ferretti, M. P. (2003). Structure and evolution of mammoth molar enamel. *Acta Palaeontologica Polonica*, *48*, 383–396.
Ferretti, M. P. (2007). Enamel structure of Cuvieronius hyodon (Proboscidea, Gomphotheriidae) with a discussion on enamel evolution in elephantoids. *Journal of Mammalian Evolution*, *15*, 37–58. https://doi.org/10.1007/s10914-007-9057-3
Fleet, M. E. (2017). Infrared spectra of carbonate apatites: Evidence for a connection between bone mineral and body fluids. *American Mineralogist*, *102*, 149–157. https://doi.org/10.2138/am-2017-5704
Fleet, M. E., Liu, X., & King, P. L. (2004). Accommodation of the carbonate ion in apatite: An FTIR and X-ray structure study of crystals synthesized at 2-4 GPa. *American Mineralogist*, *89*, 1422–1432. https://doi.org/10.2138/am-2004-1009
Garskaite, E., Gross, K.-A., Yang, S.-W., Yang, T. C.-K., Yang, J.-C., & Kareiva, A. (2014). Effect of processing conditions on the crystallinity and structure of carbonated calcium hydroxyapatite (CHAp). *Crystengcomm*, *16*, 3950–3959. https://doi.org/10.1039/c4ce00119b
Gheerbrant, E. (2009). Paleocene emergence of elephant relatives and the rapid radiation of African ungulates. *Proceedings of the National Academy of Sciences*, *106*(26), 10717–10721. https://doi.org/10.1073/pnas.0900251106
Gheerbrant, E., Bouya, B., & Amaghzaz, M. (2012). Dental and cranial anatomy of Eritherium azzouzorum from the Paleocene of Morocco, earliest known proboscidean mammal. *Palaeontographica Abteilung A*, *297*(5–6), 151–183. https://doi.org/10.1127/pala/297/2012/151
Gheerbrant, E., Sudre, J., Cappetta, H., & Bignot, G. (1998). Phosphatherium escuillieidu Thanétien du Bassin des Ouled Abdoun (Maroc), plus ancien proboscidien (Mammalia) d'Afrique. *Geobios*, *31*(2), 247–269. https://doi.org/10.1016/s0016-6995(98)80041-7
Grimes, V., & Pellegrini, M. (2013). A comparison of pretreatment methods for the analysis of phosphate oxygen isotope ratios in bioapatite. *Rapid Communications in Mass Spectrometry*, *27*(3), 375–390. https://doi.org/10.1002/rcm.6463
Halas, S., Skrzypek, G., Meier-Augenstein, W., Pelc, A., & Kemp, H. F. (2011). Inter-laboratory calibration of new silver orthophosphate comparison materials for the stable oxygen isotope analysis of phosphates. *Rapid Communications in Mass Spectrometry*, *25*, 579–584. https://doi.org/10.1002/rcm.4892
Humphrey, L. (2017). Palaeontology: Evolution with teeth. *Nature*, *545*, 26–27. https://doi.org/10.1038/545026a
Iacumin, P., Bocherens, H., Mariotti, A., & Longinelli, A. (1996). Oxygen isotope analyses of co-existing carbonate and phosphate in biogenic apatite: A way to monitor diagenetic alteration of bone phosphate? *Earth and Planetary Science Letters*, *142*, 1–6. https://doi.org/10.1016/0012-821x(96)00093-3
Klug, H. P., & Alexander, L. E. (1974). *X-ray diffraction procedures for polycrystalline and amorphous materials*. New York: Wiley-Interscience.
Kocsis, L., Gheerbrant, E., Mouflih, M., Cappetta, H., Yans, J., & Amaghzaz, M. (2014). Comprehensive stable isotope investigation of marine biogenic apatite from the late Cretaceous-early Eocene phosphate series of Morocco. *Palaeogeography, Palaeoclimatology, Palaeoecology*, *394*, 74–88. https://doi.org/10.1016/j.palaeo.2013.11.002
Koenigswald, V. W., Martin, T., & Pfretzschner, H. U. (1993). Phylogenetic interpretation of enamel structures in mammalian teeth: Possibilities and problems. In *Mammal Phylogeny* (pp. 303–314). https://doi.org/10.1007/978-1-4613-9246-0_21
Koenigswald, V. W., & Sander, P. M. (1997). Glossary of terms used for enamel microstructures. In W. V. Koenigswald, & P. M. Sander (Eds.), *Tooth enamel microstructure* (pp. 267–297). Rotterdam: Balkema.
Kohn, M. J., Schoeninger, M. J., & Barker, W. W. (1999). Altered states: Effects of diagenesis on fossil tooth chemistry. *Geochimica et Cosmochimica Acta*, *63*, 2737–2747. https://doi.org/10.1016/s0016-7037(99)00208-2
Kozawa, Y. (1978). Comparative histology of proboscidean molar enamel. *Journal of the Stomatological Society Japan*, *45*, 585–606. https://doi.org/10.5357/koubyou.45.585
Kozawa, Y. (1985). Evolution of proboscidean enamel structure. *Journal of Fossil Research*, *2*, 45–50.
Kumar, S., Bhadar, G., & Kundal, S. N. (2017). A late Pliocene Baby Stegodon cf. Stegodon insignis (Proboscidea) from Upper Siwalik of Samba District, Jammu and Kashmir, India. *Earth Science India*, *10*, 82–93. https://doi.org/10.31870/ESI.10.3.2017.7
Lee-Thorp, J. A., & van der Merwe, N. J. (1991). Aspects of the chemistry of modern and fossil biological apatites. *Journal of Archaeological Science*, *18*, 343–354. https://doi.org/10.1016/0305-4403(91)90070-6
LeGeros, R. Z. (1981). Apatites in biological systems. *Progress in Crystal Growth and Characterization*, *4*, 1–45. https://doi.org/10.1016/0146-3535(81)90046-0
LeGeros, R. Z., & Suga, S. (1980). Crystallographic nature of fluoride in enameloids of fish. *Calcified Tissue International*, *32*, 169–174. https://doi.org/10.1007/bf02408536
LeGeros, R. Z., Trautz, O. R., LeGeros, J. P., & Klein, E. (1968). Carbonate substitution in the apatite structure (1). *Bulletin de la Societe Chimique de France*, 1712–1718.
Liu, A. G. S. C., Seiffert, E. R., & Simons, E. L. (2008). Stable isotope evidence for an amphibious phase in early proboscidean evolution. *Proceedings of the National Academy of Sciences*, *105*, 5786–5791. https://doi.org/10.1073/pnas.0800884105
Locke, M. (2008). Structure of ivory. *Journal of Morphology*, *269*, 423–450. https://doi.org/10.1002/jmor.10585
Longinelli, A., & Nuti, S. (1973). Revised phosphate-water isotopic temperature scale. *Earth and Planetary Science Letters*, *19*, 373–376. https://doi.org/10.1016/0012-821x(73)90088-5
Luebke, A., Enax, J., Loza, K., Prymak, O., Gaengler, P., Fabritius, H. O., et al. (2015). Dental lessons from past to present: Ultrastructure and composition of teeth from plesiosaurs, dinosaurs, extinct and recent sharks. *RSC Advances*, *5*, 61612–61622.Link to landing page via DOI. https://doi.org/10.1039/C5RA11560D
Luebke, A., Loza, K., Patnaik, R., Enax, J., Raabe, D., Prymak, O., et al. (2017). Reply to the 'Comments on "Dental lessons from past to present: Ultrastructure and composition of teeth from plesiosaurs, dinosaurs, extinct and recent sharks"'. In, In H. Botella (Ed.),, et al., *RSC Advances*, *6*, 74384–74388. https://doi.org/10.1039/C6RA27121A
Maglio, V. J. (1973). Origin and evolution of the Elephantidae. *Transactions of the American Philosophical Society*, *63*, 1–144. https://doi.org/10.2307/1006229
Martin, C., Bentaleb, I., Kaandorp, R., Iacumin, P., & Chatri, K. (2008). Intra-tooth study of modern rhinoceros enamel δ18O: Is the difference between phosphate and carbonate δ18O a sound diagenetic test? *Palaeogeography, Palaeoclimatology, Palaeoecology*, *266*, 183–189. https://doi.org/10.1016/j.palaeo.2008.03.039
McCollum, M., & Sharpe, P. T. (2001). Evolution and development of teeth. *Journal of Anatomy*, *199*, 153–159. https://doi.org/10.1046/j.1469-7580.2001.19910153.x
Miller, H., Chenery, C., Lamb, A. L., Sloane, H., Carden, R. F., Atici, L., & Sykes, N. (2018). The relationship between the phosphate and structural carbonate fractionation of fallow deer bioapatite in tooth enamel. *Rapid Communications in Mass Spectrometry*, *33*, 151–164. https://doi.org/10.1002/rcm.8324
Nakagaki, H., Koyama, Y., Sakakibara, Y., Weatherell, J. A., & Robinson, C. (1987). Distribution of fluoride across human dental enamel, dentine and cementum. *Archives of Oral Biology*, *32*, 651–654. https://doi.org/10.1016/0003-9969(87)90039-2

Nowicki, D. A., Skakle, J. M. S., & Gibson, I. R. (2018). Nano-scale hydroxyapatite compositions for the utilization of CO2 recovered using post-combustion carbon capture. *Journal of Materials Chemistry*, *6*, 5367–5377. https://doi.org/10.1039/c7ta09334a

O'Neil, J. R., Roe, L. J., Reinhard, E., & Blake, R. E. (1994). A rapid and precise method of oxygen isotope analysis of biogenic phosphate. *Israel Journal of Earth Sciences*, *43*, 203–212.

Patnaik, R. (2016). Neogene-quaternary mammalian Paleobiogeography of the Indian Subcontinent: An appraisal. *Comptes Rendus Palevol*, *15*, 889–902. https://doi.org/10.1016/j.crpv.2015.11.004

Patnaik, R. K., Sharma, M., Mohan, L., Williams, B. A., Kay, R., & Chatrath, P. (2014). Additional vertebrate remains from the early miocene of Kutch, Gujarat. *Special Publication Of The Palaeontological Society Of India*, 353–365.

Patnaik, R., Singh Kotla, S., Premjit Singh, N., Singla, A., & Kaur, J. (2018). A new murid rodent assemblage from the Upper Siwaliks, Himachal Pradesh, India: Biostratigraphic, phylogenetic and palaeobiogeographic implications. *Journal of Asian Earth Sciences*, *162*, 93–106. https://doi.org/10.1016/j.jseaes.2017.05.030

Patnaik, R., Singh, N. P., Paul, D., & Sukumar, R. (2019). Dietary and habitat shifts in relation to climate of Neogene-Quaternary proboscideans and associated mammals of the Indian subcontinent. *Quaternary Science Reviews*, *224*, 105968. https://doi.org/10.1016/j.quascirev.2019.105968

Paul, D., Skrzypek, G., & Fórizs, I. (2007). Normalization of measured stable isotopic compositions to isotope reference scales - A review. *Rapid Communications in Mass Spectrometry*, *21*, 3006–3014. https://doi.org/10.1002/rcm.3185

Pederzani, S., Snoeck, C., Wacker, U., & Britton, K. (2020). Anion exchange resin and slow precipitation preclude the need for pretreatments in silver phosphate preparation for oxygen isotope analysis of bioapatites. *Chemical Geology*, *534*, 119455. https://doi.org/10.1016/j.chemgeo.2019.119455

Peters, F., Schwarz, K., & Epple, M. (2000). The structure of bone studied with synchrotron X-ray diffraction, X-ray absorption spectroscopy and thermal analysis. *Thermochimica Acta*, *361*, 131–138. https://doi.org/10.1016/s0040-6031(00)00554-2

Pfretzschner, H. U. (1994). Biomechanik der Schmelzmikrostruktur in den Backenzähnen von Grossäugern. Biomechanics of the enamel microstructure of large mammals. *Palaeontographica Abteilung A*, *234*, 1–88.

Puech, P.-F., Dhamelincourt, P., Taieb, M., & Serratrice, C. (1986). Laser Raman microanalysis of fossil tooth enamel. *Journal of Human Evolution*, *15*, 13–19. https://doi.org/10.1016/s0047-2484(86)80061-6

Risnes, S., & Li, C. (2019). On the method of revealing enamel structure by acid etching. Aspects of optimization and interpretation. *Microscopy Research and Technique*, *82*, 1668–1680. https://doi.org/10.1002/jemt.23333

Roca, A. L., Georgiadis, N., Pecon-Slattery, J., & O'Brien, S. J. (2001). Genetic evidence for two species of elephant in Africa. *Science*, *293*, 1473–1477. https://doi.org/10.1126/science.1059936

Roche, D., Ségalen, L., Balan, E., & Delattre, S. (2010). Preservation assessment of Miocene-Pliocene tooth enamel from Tugen Hills (Kenyan Rift Valley) through FTIR, chemical and stable-isotope analyses. *Journal of Archaeological Science*, *37*, 1690–1699. https://doi.org/10.1016/j.jas.2010.01.029

Rögl, F. (1998). Palaeogeographic considerations for mediterranean and paratethys seaways (Oligocene to Miocene). 99A, 279–310. AnnalendesNaturhistorischenMuseumsinWien

Sakae, T., Mishima, H., & Kozawa, Y. (1991). Proboscidea fossil teeth suggest the evolution of enamel crystals. *Mechanisms and Phylogeny of Mineralization in Biological Systems*, 477–481. https://doi.org/10.1007/978-4-431-68132-8_76

Stephan, E. (2000). Oxygen isotope analysis of animal bone phosphate: Method refinement, influence of consolidants, and reconstruction of palaeotemperatures for holocene sites. *Journal of Archaeological Science*, *27*, 523–535. https://doi.org/10.1006/jasc.1999.0480

Tabuce, R., Delmer, C., & Gheerbrant, E. (2007). Evolution of the tooth enamel microstructure in the earliest proboscideans (Mammalia). *Zoological Journal of the Linnean Society*, *149*, 611–628. https://doi.org/10.1111/j.1096-3642.2007.00272.x

Teaford, M. F., Smith, M. M., & Ferguson, M. W. J. (2000). *Development, function and evolution of teeth*. Cambridge: Cambridge University Press.

Van der Made, J. (2010). The evolution of the elephants and their relatives in the context of changing climate and geography. In D. Höhne, & W. Schwarz (Eds.), *Elefantenreich - Eine Fossilwelt in Europa* (pp. 340–360). Halle, Germany: Landesamt für Denkmalpflege und Archäologie Sachsen-Anhalt & Landesmuseum für Vorgeschichte.

Vollrath, F., Mi, R., & Shah, D. U. (2018). Ivory as an important model bio-composite. *Curator: The Museum Journal*, *61*(1), 95–110. https://doi.org/10.1111/cura.12236

Wilmers, J., & Bargmann, S. (2020). Nature's design solutions in dental enamel: Uniting high strength and extreme damage resistance. *Acta Biomaterialia*, *107*, 1–24. https://doi.org/10.1016/j.actbio.2020.02.019

Wu, Y., Deng, T., Hu, Y., Ma, J., Zhou, X., Mao, L., et al. (2018). A grazing Gomphotherium in middle Miocene Central Asia, 10 million years prior to the origin of the Elephantidae. *Scientific Reports*, *8*, 7640. https://doi.org/10.1038/s41598-018-25909-4

Zazzo, A., Lécuyer, C., & Mariotti, A. (2004). Experimentally-controlled carbon and oxygen isotope exchange between bioapatites and water under inorganic and microbially-mediated conditions. *Geochimica et Cosmochimica Acta*, *68*(1), 1–12. https://doi.org/10.1016/s0016-7037(03)00278-3

Zazzo, A., Lécuyer, C., Sheppard, S. M. F., Grandjean, P., & Mariotti, A. (2004). Diagenesis and the reconstruction of paleoenvironments: A method to restore original δ18O values of carbonate and phosphate from fossil tooth enamel. *Geochimica et Cosmochimica Acta*, *68*, 2245–2258. https://doi.org/10.1016/j.gca.2003.11.009